Available online at www.sciencedirect.com
ScienceDirect
Trans. Nonferrous Met. Soc. China 20(2010) 1899−1905
Transactions of Nonferrous Metals Society of China
www.tnmsc.cn

Electrode properties and phase composition of $Ti_{0.5}Ni_{0.25}Al_{0.25}$ hydrogen storage alloys and theoretical simulation

WU Jun(吴 军)[1], XU Yan-hui(徐艳辉)[1], CHEN Chang-pin(陈长聘)[2],
ZHENG Jun-wei(郑军伟)[1], LI De-cheng(李德成)[1]

1. Institute of Electrochemical Power Sources, Soochow University, Suzhou 215006 China;
2. Department of Materials Science and Engineering, Zhejiang University, Hangzhou 310027, China

Received 12 October 2009; accepted 22 February 2010

Abstract: $Ti_{0.5}Al_{0.25}Ni_{0.25}$ alloy prepared by vacuum induction melting was studied. The phase composition was analyzed with X-ray technique and EDS analysis, and its electrochemical properties were investigated at various temperatures. Electrochemical reaction kinetic parameters were also studied with proper electrochemical techniques. The influence of the secondary corrosion reaction on the anodic linear polarization measurement was also analyzed by theoretical simulation. The results show that, proper ball-milling with nickel powders is beneficial to electrochemical performance. The theoretical simulation proves that, the existence of the side reaction can disturb the measurement of electrochemical reaction kinetic parameters.
Key words: hydrogen storage alloy; electrochemical kinetics; metal hydride electrode; theoretical simulation

1 Introduction

Among all the factors promoting the scientists to study and improve electrochemical behavior of rechargeable secondary battery, the commercial purpose is one of the main drivers. The consciousness on the energy crisis accelerates the research progress, the evidence of which is increased number of scientific articles have been published. Recently, the main secondary battery includes lithium-ion, acid lead and nickel-metal hydride secondary batteries, which occupy the different application fields and cannot replace each other. Many researchers attempt to improve the electrochemical behavior of positive and negative electrodes of Ni-MH battery[1−7]. Among them, the negative electrode metal hydride materials are more attractive due to their variety: AB_5-type rare-earth alloy[1, 3], AB_2 Laves alloy[4, 8−9], V-based solid solution alloy[5], Ti-Ni series[7, 10], AB_3-type rare-earth alloy[11−12], etc. Ti_3Al has a DO19 hexagonal structure; after being charged, the formed hexagonal hydride has parameters of a=0.585 8 nm and c=0.465 7 nm. SORNADURI et al[13] found that the phase structure of the formed hydride prepared by electrochemical charge is different from that prepared by gas-phase reaction: the hydride formed by gas-phase reaction is of cubic structure. RUDMAN et al[14] observed that this material has hydrogen storage of 1.5 H/M, corresponding to a theoretical capacity of 942 mA·h/g. The formation entropy is −127.28 J/mol and the formation enthalpy is −47.31 J/mol H_2. The pressure−composition−temperature measurement (PCT curve) has shown a plateau of less than 10^5 Pa at 323 K and $(1−2)\times10^5$ Pa at 373 K. A disadvantage is that the formation of γ-hydride phase is irreversible. The crystal parameters of Ti_3Al alloy are listed in Table 1.

As mentioned above, at 373 K the pressure plateau is about 10^5 Pa; the composition elements Ti and Al are light metal. From the view point of thermodynamics, it is suitable for application in high-temperature Ni-MH battery. Considering that for electrochemical application the high electro-catalytic activity was required, proper amount of nickel element was introduced into the alloy. As an exploratory research, the $Ti_{0.5}Ni_{0.25}Al_{0.25}$ alloy was designed and investigated regarding its electrochemical behavior.

Corresponding author: XU Yan-hui; Tel: +86-512-67261337; E-mail: xuyanhui@suda.edu.cn, xu.juxiaomeng@gmail.com
DOI: 10.1016/S1003-6326(09)60392-7

Table 1 Phase structure and parameters of crystal unit cell of Ti_3Al-H system

Phase	Structure	Lattice parameter/Å	$x=n(H):n(M)$	V/Å^3	$x_f=n(H):n(M)$
α	A3 HCP	a=2.89, c=4.66	0−2	16.85	0
β	A2 BCC	a=3.28	0.49	17.66	0.35
γ	A1 FCC	a=4.35	1.26	20.54	1.6
α(Ti)	A3 HCP	a=2.952, c=4.689	−	17.69	0
$\gamma(TiH_2)$	A1 FCC	a=4.46	−	2.18	2

2 Experimental

The purities of all used original metals were more than 99.5% (mass fraction). A vacuum induction melting was used; metal Al had an excess of 15%. The prepared alloy had a large brittleness and was easy to be ground to a powder. The milling procedure was as follows. 4.0 g of alloy powders was put into a jar of 250 mL, the mass of the used balls was 5 g and the mass ratio of the balls to alloy was 20:1. The nickel powder added into the alloy was 2.5% and 7.5% (mass fraction) and the rotating rate was 200 r/min. The mixture of alloy powders and nickel powders (mass ratio is 1:2) was pressed at 1.0 MPa to form a round disk for electrochemical test. The counter electrode is the commercial nickel electrode and the reference electrode is Hg/HgO electrode. The more details can be seen in Ref.[8].

3 Results and discussion

3.1 Electrochemical properties

The charge−discharge curves of the as-cast alloy and the alloys milled for 20 h are shown in Fig.1. Increasing the ambient temperature from 300 K up to 353 K causes the potential plateau to be more slantwise and unclear. Electrode potential increases rapidly up to the potential at which the water starts to decompose. These phenomena imply that the increase of the ambient temperature will decrease the columbic efficiency of the charge. But increasing temperature is good for the discharge capacity.

Ball-milling leads to the decrease of the alloy electrode capacity. For the sample with no nickel powder at 300 K, when the ball milling time increases from 20 to 60 h, the discharge capacity decreases by 15 and 25 mA·h/g, while at 353 K the discharge capacity decreases by 48 mA·h/g. For the sample with 2.5% nickel powder ball-milled for 60 h, its discharge capacity is less than that of the as-cast alloy; but at 323 K its discharge capacity reaches 160.5 mA·h/g, a little more than 157 mA·h/g of the as-cast alloy. For the sample with 7.5% nickel powder milled for 60 h, its discharge capacity decreases at 300 and 323 K but increases at 353 K. Increasing the milling time up to 108 h will improve the discharge capacity at 300 K (from 110 to 127 mA·h/g), but decrease from 227 to 184 mA·h/g at 353 K.

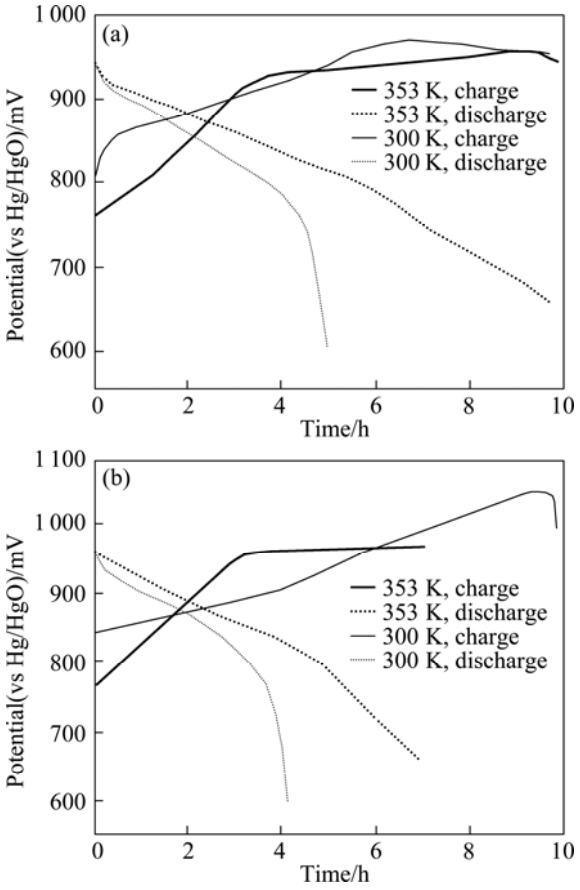

Fig.1 Discharge−charge curves of as-cast alloy (a) and alloy milled for 20 h (b) at charge current of 50 mA/g and discharge currvent of 20 mA/g

The influence of ball-milling parameters on the discharge is shown in Fig.2. Regardless of whether ball-milling or not, at 353 K the discharge curve is composed of two potential plateaus: a declining plateau in the region from −790 to −890 mV and a plateau at ~−700 mV with a smaller capacity. At 300 K, there is only one plateau. The existence of two plateaus implies that there are at least two hydride phases in the charging state. Because every hydride has a different discharge potential, there are two potential plateaus at 353 K; but at 300 K, the corresponding pressure plateau on its gaseous PCT curves is so low that the stored hydrogen cannot be released when the final discharge potential is set at −0.6 V. The electrochemical discharge capacity is related to its

pressure plateau on the gaseous PCT curve. The temperature influences the pressure plateau on its PCT curve, therefore influences the discharge capacity of the corresponding electrode alloy. Fig.3 shows the maximum discharge capacity of the as-cast and milled alloy electrodes at 300, 323 and 353 K when the discharge current is 25 mA/g. As the temperature increases, the discharge capacity increases, which also implies their relatively low pressure plateau on the corresponding PCT curves. The discharge capacities of the as-cast alloy are 138, 157 and 279 mA·h/g at 300, 323 and 353 K, respectively. The reversible capacity is much less than the theoretical capacity.

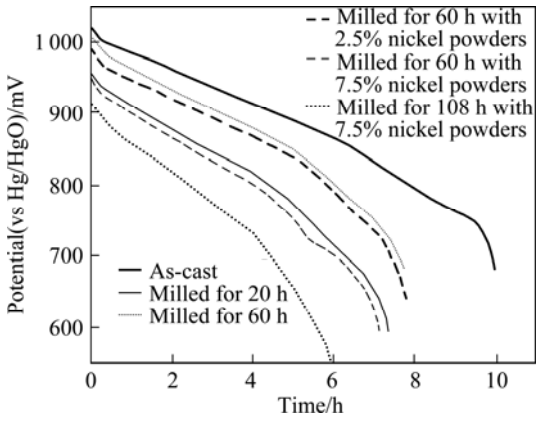

Fig.2 Discharge curves of as-cast and milled alloys at 353 K

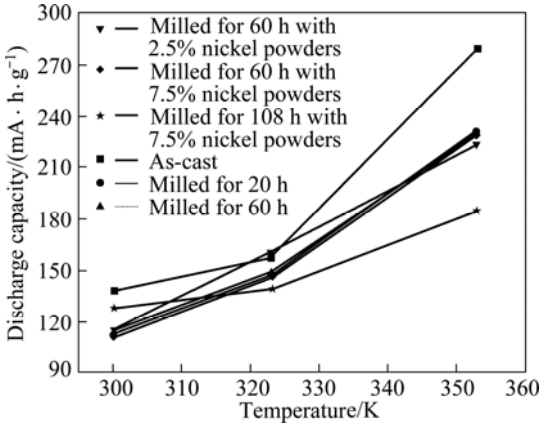

Fig.3 Maximum capacity of alloy electrodes at various temperatures

Cycling capacities of $Ti_{0.5}Ni_{0.25}Al_{0.25}$ alloy electrodes at different temperatures are shown in Figs.4−6. From Fig.4, at 353 K, after 30 cycles, the discharge capacity of ball-milled alloy is larger than that of the as-cast alloy; the capacity of the alloy milled with nickel powder is even larger. This shows that ball-milling, especially with nickel powder, is effective to improve the cycling stability at 353 K. But it can be seen from Figs.5 and 6 that, cycling life becomes poorer at 300 and 323 K. For example, at 323 K, the discharge capacity of the as-cast alloy decreases from 157 to 130 mA·h/g after 40 cycles, while the capacity of the ball-milled alloy is less than 100 mA·h/g and its capacity conservation is less than 67%. The above mentioned analyses confirm that the long-term milling (> 20 h) is bad to cycling life at 300 and 323 K.

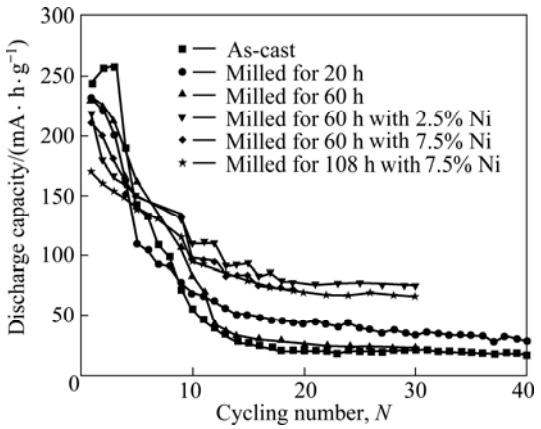

Fig.4 Cycling capacity of $Ti_{0.5}Ni_{0.25}Al_{0.25}$ alloy electrodes at 353 K

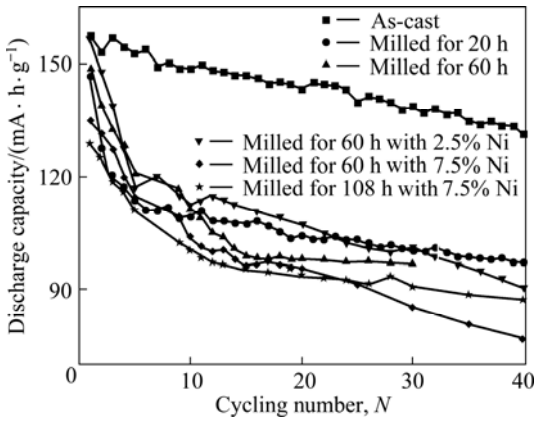

Fig.5 Cycling capacity of $Ti_{0.5}Ni_{0.25}Al_{0.25}$ alloy electrodes at 323 K

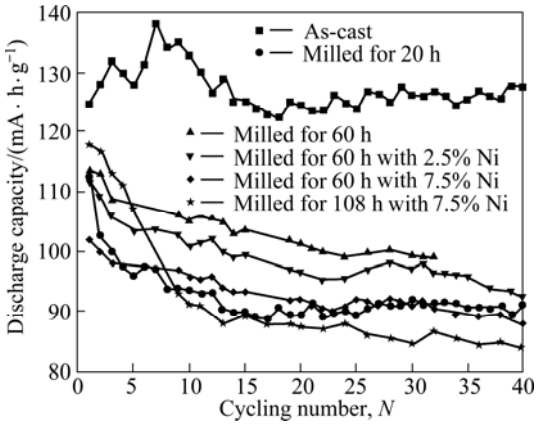

Fig.6 Cycling capacity of $Ti_{0.5}Ni_{0.25}Al_{0.25}$ alloy electrodes at 300 K

The activation can be improved by the ball-milling treatment at 300 K. The activation number of the as-cast alloy is 7 but after ball-milling for 20 h it is only 2. For the ball-milled sample the maximum capacity is reached at the first cycle. It is still found that increasing the temperature can improve the activation but decrease the cycling stability.

3.2 Phase composition analysis

The phase composition analysis was conducted with X-ray diffraction technique. From Fig.7, it can be determined that the alloy is composed of CsCl-type cubic NiTi phase, cubic Ti_2Ni phase, hexagonal Ti_2Al phase, tetragonal $Ti_8(TiAl_{23})$ phase, and other impurity phase which is difficult to be defined. After corrosion pretreatment, there are corrosion pits on the surface and no dendrite crystal or isometric crystal is found.

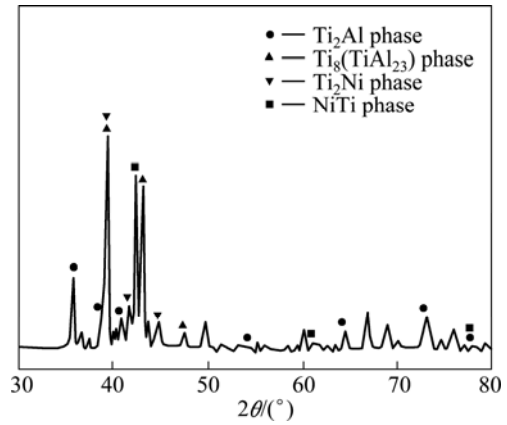

Fig.7 XRD pattern of as-cast $Ti_{0.5}Ni_{0.25}Al_{0.25}$ alloy

Figs.8(a) and (b) show the SEM image and EDS pattern of as-cast $Ti_{0.5}Ni_{0.25}Al_{0.25}$ alloy after being corroded. Pattern 1 shows the bright dot, pattern 2 shows the gray region, and patterns 2 and 3 show the dark region in Fig.8(a), respectively. The EDS results show that the Al content decreases from the alloy bulk to the grain boundary while the Ti content increases, i.e., the element Ti segregates and gathers at the grain boundary. After ball-milling, the XRD patterns of the alloys are shown in Fig.9. Ball-milling causes poor crystallinity; the diffraction peaks of $Ti_8(TiAl_{23})$, NiTi and Ti_2Al phases become weak, and the ones of other phases disappear. After milling, the main peaks of $Ti_8(TiAl_{23})$ and Ti_2Al phases shift to larger diffraction angle, while the main peaks of NiTi phases and the peaks that correspond to (0016) plane of $Ti_8(TiAl_{23})$ phase shift to smaller diffraction angle. The different phases have a tendency to syncretize. For the sample with 2.5% nickel powder ball-milled for 60 h, no diffraction peak is found that corresponds to the metal nickel, which implies that the added nickel powder is mixed into other phase or is amorphous or is nano-crystal. For the sample with 7.5% nickel powder, if the ball-milling time is set at 60 h, there exists metal nickel in the alloy; while if the ball-milling time is 108 h, in the XRD pattern there is no peak that corresponds to metal nickel. Of all the samples ball-milled, as mentioned above, the sample with 7.5% nickel powder milled for 60 h is composed of bulk alloy with poor crystallinity and little amount of metal nickel. At the same time, this alloy has relatively high electrochemical capacity and good high-rate discharge ability (HRD). It seems that the little amount of metal nickel plays a key role to improve the electro-catalytic activity and the bulk alloy acts as the storehouse to store the hydrogen. This result may confirm that for electrochemical application, the proper amount of metal nickel is necessary to ensure the electrochemical properties. The contact between bulk alloy phase and metal nickel powders should be compact to ensure the mass transportation.

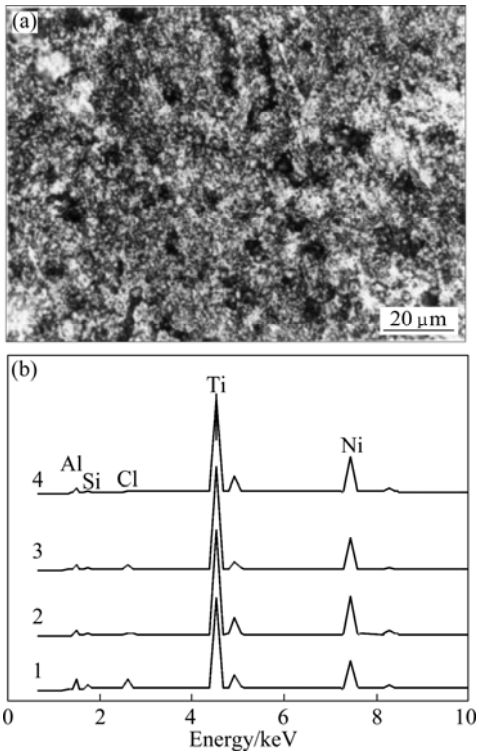

Fig.8 SEM image (a) and EDS pattern (b) of as-cast $Ti_{0.5}Al_{0.25}Ni_{0.25}$ alloy

The crystal grain size of ball-milled $Ti_{0.5}Ni_{0.25}Al_{0.25}$ alloy can be calculated with the following equation:

$$L=\frac{k\lambda}{\beta\cos\theta} \tag{1}$$

where β is the peak width at half height, λ is the wave length, θ is the diffraction angle. In general, the k value is to be 1. From Fig.9, the peak width at half height β is 1°−1.5°, therefore the crystal grain is about 10−15 nm in size.

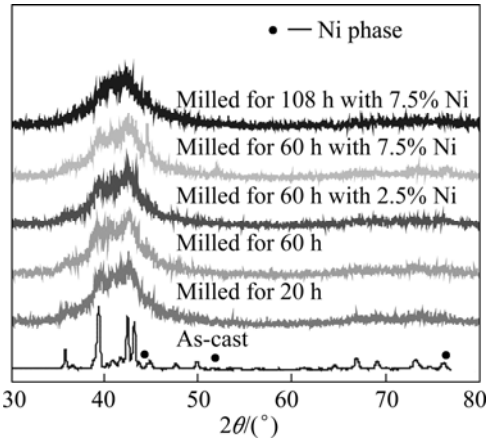

Fig.9 XRD pattern of $Ti_{0.5}Ni_{0.25}Al_{0.25}$ alloys

3.3 Reaction kinetic parameters

The corresponding electrochemical kinetic parameters have been measured, as shown in Table 1. The apparent exchange current can be obtained by linearizing the equation when the over potential is less than 10 mV:

$$\eta = \frac{RT}{I^0 nF} I \tag{2}$$

where η is the over potential, T is the temperature, I is the measured current, n is the exchanged electron number, I^0 is the exchange current.

The activation energy E^0 for electron exchange reaction on the electrode surface can be calculated by Eq.(3) as follows[15]:

$$I^0 = A\exp[-E^0/(RT)] \tag{3}$$

Another method was presented to calculate the exchange current [16−17]:

$$\eta = \frac{RT}{(1-\alpha)nF}\ln\frac{I_L}{I^0} + \frac{RT}{(1-\alpha)nF}\ln\left(\frac{I}{I_L - I}\right) \tag{4}$$

Plotting the over potential vs $\ln\left(\frac{I}{I_L - I}\right)$, the exchange current can be calculated using the intercept, and the energy transportation coefficient α can be also calculated at same time.

The apparent proton diffusion coefficient D can be calculated by the following expression[18−19]:

$$D = \frac{r_0^2 I}{15(Q_0 - I\tau)} \tag{5}$$

where I is the discharge current, r_0 is the average radius of the alloy grain, Q_0 is the maximum capacity when the discharge current is I, τ is the transition time.

All the parameters are listed in Table 2. It can be found that the ball-milling causes the apparent exchange current to increase and the electro-catalytic activity of the alloy electrode surface is improved by the ball-milling treatment. In addition, adding little amount of nickel powder to ball-milling is more effective to increase the electro-catalytic activity. This is believed to be related to the nickel nature. After ball-milling the alloy powder together with the nickel powders, free nano-sized nickel powder is adhered tightly on the alloy surface and the surface layer with rich nickel is formed. It can be still seen from the Table 1 that, the energy transition coefficient is clearly far from 0.5, so the influence of the polarization on the cathode and anode reactions is different. The apparent activation energy of the exchange reaction is decreased for the ball-milled alloys, especially with added nickel powder. The activation energy for the as-cast alloy is 14.2 kJ/mol while after being ball-milled with nickel powder, which can be decreased to less than 5 kJ/mol.

The apparent proton diffusion coefficient D of the as-cast alloy is 1.33×10^{-9} cm^2/s. After ball-milling from 20 to 60 h, the D value increases from 1.46×10^{-9} to 1.97×10^{-9} cm^2/s. The longer term of ball-milling causes the D value to be decreased (for 108 h, the D value is 0.98×10^{-9} cm^2/s). The influence of the added nickel powder during ball-milling is relatively complex. The purpose is to ball-mill the alloy with nickel powder to make the free nickel powder to be adhered closely and

Table 2 Electrochemical kinetic parameters of $Ti_{0.5}Ni_{0.25}Al_{0.25}$ alloy electrodes

Alloy	$D_{300\ K}$ / (10^{-9}cm^2·s^{-1})	R_L/(Ω·g)		$I^0_{300\ K}$ /(mA·g^{-1}) *,	$\alpha_{300\ K}$	I^0/(mA·g^{-1})**		E^0/ (kJ·mol^{-1})	$I_{L,300\ K}$ / (mA·g^{-1})
		300 K	323 K			300 K	323 K		
As-cast	1.33	0.460	0.332	36.84	0.36	56.0	84.0	14.2	426.6
Milled for 20 h	1.46	0.425	0.281	55.77	0.37	61.0	99.0	17.0	468.8
Milled for 60 h	1.97	0.295	0.271	54.69	0.35	88.0	103.0	5.50	478.9
Milled for 60 h with 2.5% Ni	1.79	0.229	0.235	86.40	0.39	113.0	118.0	1.52	510.2
Milled for 60 h with 7.5% Ni	2.34	0.245	0.273	71.11	0.25	105.0	120.5	4.80	542.6
Milled for 108 h with 7.5% Ni	0.98	0.302	0.290	78.10	0.40	86.0	96.0	3.85	494.0

*calculated from equation 4; **calculated using equation 2

compactly on the alloy grain surface. To adhere compactly is to ensure the mass transportation, while the formation of the nickel-rich surface is to ensure the electro-catalytic activity.

In Table 2, the apparent activation energy of exchange reaction is calculated using the exchange current that is measured with linear polarization method. It is necessary to discuss why the exchange current data calculated from Eq.(4) is not used for calculating the activation energy. When the anode linear polarization measurement is conducted, the secondary reaction is not avoided the corrosion reaction of the alloy. We need to know how the corrosion reaction influences the linear polarization measurement of metal hydride electrode. The simulation of the linear polarization curve can solve and answer this problem.

3.4 Theoretical simulation

The discharge process of hydrogen storage alloy electrode can be expressed by the following steps.

1) The hydrogen diffusion in the bulk alloy. At same time, the following phase transition process may take place: $H_{abs,\ bulk} \rightleftharpoons H_{abs,\ surface}$, $MH_{phase1} \rightleftharpoons MH_{phase2}$.

2) From the absorbed state to the adsorbed state: $H_{abs,\ surface} \rightleftharpoons H_{ads,\ surface}$.

3) Surface electrochemical reaction: $H_{ads,\ surface} + OH^- \rightleftharpoons H_2O + e$.

4) The transportation process of the formed water and the OH^- ions: $H_2O_{double\text{-}layer} \rightleftharpoons H_2O_{solution}$, $OH^-_{solution} \rightleftharpoons OH^-_{double\text{-}layer}$

Here, we will discuss the influence of the corrosion reaction on the limiting current measurement. Therefore, the electrochemical process is considered to be controlled by the diffusion process and surface electron exchange process. The simulation equation is as follows:

$$I = I^0\left\{\exp\left(\frac{\alpha nF}{RT}\eta\right) - \exp\left(-\frac{(1-\alpha)nF}{RT}\eta\right)\right\} \tag{6}$$

$$\eta = \frac{RT}{nF}\ln\frac{I_L}{I_L - I} \tag{7}$$

The corrosion process of the alloy is believed to be controlled only by the mass transportation process. If there is a corrosion process, then the total current I is divided into two parts: Faraday current I_F and corrosion current I_{corr}: $I=I_F+I_{corr}$. The simulation calculation of I_{corr} is assumed that the corrosion reaction is controlled by the mass transportation process. The simulation result is shown in Fig.10. Curve (b) in Fig.10 represents the theoretical polarization curve of alloy electrode without the disturbing of corrosion reaction; curve (b) in Fig.10 shows the polarization curve when the two reactions coexist. It can be concluded that, the existence of the secondary corrosion reaction must lead to the fact that the measured limiting current is much larger than the true value. Therefore, in Table 1, when we calculate the activation energy we use the exchange current data coming from the Eq.(2). The simulation results confirm that, it should be cautious to use the limiting current measurement method that is usually used in electrochemical system (i.e., linear polarization method). The directly measured limiting current data are much larger than the true values.

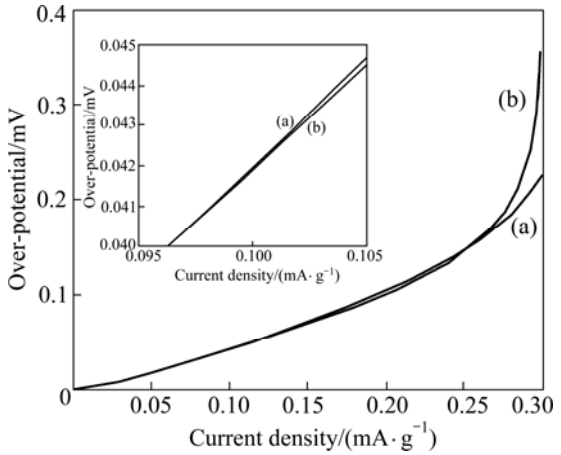

Fig.10 Simulated linear polarization curves: (a) With corrosion reaction; (b) Without corrosion reaction

4 Conclusions

1) Proper ball-milling with nickel powders can improve its electrochemical performance, but the perfect ball-milling condition needs a further investigation.

2) The effect of the secondary corrosion reaction of the alloy on the linear polarization measurement was studied and the results show that, because of the disturbance of this corrosion reaction, the directly obtained limiting current from the measured linear anodic polarization curve is larger than the true value.

References

[1] UCHIDA H, MATSUMOTO T, WATANABE S, KOBAYASHI K, HOSHINO H. A paste type negative electrode using a $MmNi_5$ based hydrogen storage alloy for a nickel-metal hydride (Ni-MH) battery[J]. International Journal of Hydrogen Energy, 2001, 26(7): 735−739.

[2] XU Yan-hui, CHEN Chang-pin, LI Shou-quan, YING Tiao, WANG Qi-dong. High-temperature electrochemical performance and phase composition of $Ti_{0.7}Zr_{0.5}V_{0.2}Mn_{1.8-x}Ni_x$ hydrogen storage alloys [J]. Transactions of Nonferrous Metals Society of China, 2001, 11(3): 350−352.

[3] XU Yan-hui, JU Hua. The structure, thermodynamic and electrochemical properties of hydrogen-storage alloys: An empirical methodology of average numbers of total electrons[J]. International Journal of Hydrogen Energy, 2009, 34(4): 1880−1885.

[4] XU Yan-hui, CHEN Chang-pin, WANG Xiao-lin, WANG Qi-dong. The hydrogen evolution reaction during charging for Ti-Zr-V-Ni-Cr alloy electrode[J]. International Journal of Hydrogen Energy, 2007, 32(5): 537−541.

[5] TSUKAHARA M, TAKAHASHI K, ISOMURA A, SAKAI T. Influence of oxygen on hydrogen storage and electrode properties for micro-designed V-based battery alloys[J]. Journal of Alloys and Compounds, 1998, 265(1/2): 257−263.

[6] CARINE R, LIONEL R. Effect of particle size on the electrode performance of MgNi hydrogen storage alloy[J]. Journal of Power Sources, 2004, 132(1/2): 302−308.

[7] XU Yan-hui, CHEN Chang-pin, WANG Qi-dong, CHEN Li-xin. The effect of temperature on the electrode properties of the directly prepared Ti_3Ni_2 alloy[J]. International Journal of Hydrogen Energy, 2001, 26(11): 1177−1181.

[8] XU Yan-hui, CHEN Chang-pin, WANG Xiao-lin, WANG Qi-dong. The structure and electrochemical properties of ball-milled $Ti_{0.9}Zr_{0.2}Mn_{1.6}Ni_{0.2}V_{0.2}$ alloys[J]. Solid State Ionics, 2002, 146(1/2): 157−161.

[9] KNOSP B, VALLET L, BLANCHARD P H. Performance of an AB_2 alloy in sealed Ni-MH batteries for electric vehicles: Quantification of corrosion rate and consequences on the battery performance[J]. Journal of Alloys and Compounds, 1999, 293/294/295: 770−774.

[10] LUAN B, CUI N, ZHAO H J, LIU H K, DOU S X. Effects of potassium-boron addition on the performance of titanium based hydrogen storage alloy electrodes[J]. International Journal of Hydrogen Energy, 1996, 21(5): 373−379.

[11] ZHAO Xian-jiu, LI Qian, LIN Gen-wen; CHOU Kuo-chih. Effects of magnetic-heat treatment on microstructure and electrochemical properties of La-Mg-Ni-Co alloys[J]. The Chinese Journal of Nonferrous Metals, 2008, 18(11): 2030−2035.(in Chiaese)

[12] LI F, YOUNG K, OUCHI T, FETCENKO M A. Annealing effects on structural and electrochemical properties of $(LaPrNdZr)_{0.83}Mg_{0.17}(NiCoAlMn)_{3.3}$ alloy[J]. Journal of Alloys and Compounds, 2009, 471(1/2): 371−377.

[13] SORNADURAI D, PANIGRAHI B K, SASTRY V S. Highly oriented hexagonal hydride phase formation in single phase Ti_3Al by cathodic charging[J]. Journal of Alloys and Compounds, 1999, 289(1/2): L1−L5.

[14] RUDMAN P S, REILLY J J, WISWALL R H. The formation of metastable hydrides $Ti_{0.75}Al_{0.25}H_x$ with $x < 1.5$[J]. Journal of the Less Common Metals, 1978, 58(2): 231−240.

[15] HIDEKI Y, AKIHISA T, KAZUYOSHI H. Activation energies for electrode reaction of metal hydride in alkaline aqueous solution[J]. Jpn J Appl Phys 1989, 28: 530−534.

[16] WU Mao-sung, WU Hong-rong, WANG Yung-yun, WAN Chi-chao. Surface treatment for hydrogen storage alloy of nickel/metal hydride battery[J]. Journal of Alloys and Compounds, 2000, 302(1/2): 248−257.

[17] XU Yan-hui, CHEN Chang-pin, WANG Xiao-lin, WANG Qi-dong. The relationship between the high-rate dischargeability and the diffusion coefficient and exchange current for $Ti_{0.5}Ni_{0.25}Al_{0.25}$ metal hydride alloys[J]. Journal of Alloys and Compounds, 2002, 335(1/2): 262−265.

[18] XU Yan-hui, WANG Guo-yuan, CHEN Chang-pin, WANG Qi-dong, WANG Xiao-lin. The structure and electrode properties of non-stoichiometric $A_{1.2}B_2$ type C14 Laves alloy and the effect of surface modification[J]. International Journal of Hydrogen Energy, 2007, 32(8): 1050−1058.

[19] XU Yan-hui, CHEN Chang-pin, WANG Qi-dong. The influence of small amounts of added elements on the electrode performance characteristics for Ti_3Ni_2 hydrogen storage alloy[J]. Materials Chemistry and Physics, 2001, 71(2): 190−194.

(Edited by LI Xiang-qun)